Finite-size effects in ionization potentials and electron affinities of metal clusters

M. Seidl
Institut für Theoretische Physik, Universität Regensburg, D 8400 Regensburg, Germany

K.-H. Meiwes-Broer
Fakultät für Physik, Universität Bielefeld, D 4800 Bielefeld 1, Germany

M. Brack
Institut für Theoretische Physik, Universität Regensburg, D 8400, Regensburg, Germany

(Received 31 January 1991; accepted 29 March 1991)

Experimental ionization potentials (I) and electron affinities (A) of metal clusters Me_N are compiled for a variety of systems and their size dependence is analyzed. In the theoretical part, we perform semiclassical density variational calculations using the spherical jellium model and the local density approximation. For alkali systems and, to some extent, also for some nonalkali systems, the calculated values of I and A reproduce very well the average size dependence of the measured quantities, if their common bulk limit W is adjusted to the experimental bulk work function. This holds even for rather small systems where I and A are no longer linear in $N^{-1/3}$. We discuss the extent to which classical models for the energetics of charged metal spheres can account for the correct size dependence in the large-cluster limit. We point out that the deviation of the slope parameters α and β in the asymptotic expressions $I \sim W + \alpha(e^2/r_s)N^{-1/3}$, $A \sim W - \beta(e^2/r_s)N^{-1/3}$ from the values $\frac{1}{2}$, which depends on the material via the Wigner–Seitz parameter r_s, can be entirely accounted for by quantum-mechanical effects, namely the kinetic, exchange, and correlation energies and the diffuseness of the electron density.

I. INTRODUCTION

Small atomic aggregates are receiving an increasing interest both in basic and applied sciences. The confinement of a metal to a small volume gives rise to significant deviations of its physical and chemical properties from their respective bulk characteristics. In the case of alkali and alkalilike clusters, the most pronounced confinement effects are: (i) a size dependence of observables such as ionization potential, electron affinity, or static dipole polarizability; and (ii) pronounced shell effects in ionization and binding energies, especially at or near the so-called "magic numbers" of valence electrons. (See, e.g., a recent review on metal clusters.)[1]

A completely microscopic *ab initio* description[2] of microclusters is certainly adequate, but restricted to the smallest systems only. On the other hand, density functional theory in local density approximation (LDA) using the spherical[3-6] or ellipsoidal[7] *jellium model* has been able to account semiquantitatively for the abovementioned phenomena—in spite of its enormous simplifications neglecting the microscopic structure and dynamics of the atoms (including the core electrons)—in terms of a mean potential felt by the valence electrons. In particular, the increased stability of alkali clusters with a magic number N of atoms finds its natural explanation in the closure of spherical shells in the electronic single-particle spectrum. These magic numbers have now been observed[8,9] up to $N \sim 600$ or even $N \sim 1400$ (depending on the experimental technique) and can also be more or less correctly calculated up to these sizes using both phenomenological[10] and self-consistent[9,11] jellium model potentials.

Besides these observations of increased stability, recent experimental work on metal clusters has also yielded extensive amounts of other data on, e.g., ionization potentials, electron affinities, and reactivities. Even electronically excited states of neutral and ionized clusters are accessible to the experiment (see, e.g., two recent conference proceedings).[12,13]

In this communication, we concentrate on the size dependence of the (first) ionization potential I and electron affinity A, defined in terms of the total energy $E(N,z)$ of a cluster with N atoms and z excess electrons by

$$I = E(N,-1) - E(N,0), \quad A = E(N,0) - E(N,+1). \tag{1}$$

We have compiled experimental data for a variety of simple metals, both alkalis and others, and shall compare them to the results of variational jellium model calculations in a recently developed semiclassical approximation.[14] In particular, we shall also discuss their asymptotic behavior for large clusters.

The jellium model is known[3-7] to overemphasize the observed shell-structure oscillations in I and A. We therefore have chosen here the approach of Ref. 14 which ignores shell effects from the beginning, but has been shown to reproduce very well *on the average* all properties found in microscopic jellium model calculations. This allows us particularly well to investigate large clusters with N up to $\sim 10^6$ and to extract the exact asymptotic limits of the quantities of interest.

It has been suggested for a long time[15,16] that apart from the shell structure oscillations, the ionization potential I and the electron affinity A should both converge to the bulk work

 0021-9606/91/141295-09$03.00

function W as N tends to infinity. It is therefore very useful to expand the N dependence of I and A asymptotically as

$$I(N) = W_I + \alpha \frac{e^2}{R_I} + O(R_I^{-2}), \tag{2}$$

$$A(N) = W_A - \beta \frac{e^2}{R_I} + O(R_I^{-2}), \tag{3}$$

where R_I is the radius of the sharp-edged jellium sphere

$$R_I = r_s N^{1/3}, \tag{4}$$

r_s being the Wigner–Seitz radius which characterizes the ionic lattice of the corresponding bulk metal. From theoretical considerations (see Sec. V), W_I and W_A should be equal and identical to W.

There exists quite an abundance of literature about the values of the parameters α and β in Eqs. (2) and (3). Experimentally, most data on I suggest[17,18] a value of $\alpha \simeq \frac{1}{8}$, whereas the data on A seem to prefer[19–21] a value of $\beta \simeq \frac{5}{8}$. However, in most experimental fits, Eqs. (2) and (3) were truncated after the second term by plotting I and A vs $N^{-1/3}$ or $1/R_I$ and drawing a *straight* line through the data, cutting the ordinate at the experimental value W_{bulk}. Also, in order to simulate effects of the spillout of the electronic density beyond the cluster (jellium) edge, the radius R_I was either replaced by some experimental value or changed by adding to Eq. (4) a more or less *ad hoc* constant. Furthermore, the shell effects which are not contained in Eqs. (2) and (3) often obliterate the possibility of extracting unique slopes α and β of such plots, especially when data only of small clusters are available. Taking finally an account of the uncertainty in some of the experimental bulk work functions W_{bulk}, we are left with rather large error bars in the experimental values of the slope parameters α and β.

As to the theoretical predictions[15,16,22–27] of these slope parameters, they vary between $\alpha = \frac{1}{3}$, $\beta = \frac{5}{8}$, and a common value of $\frac{1}{2}$ for both. Unfortunately, there still remains in the literature a confusing controversy about their values expected from purely classical considerations, to which we will return in Sec. V of this paper. Let us just anticipate here that quantum-mechanical effects contribute to the slope parameters as well as they influence the bulk work function W. (The latter is, in fact, zero in a classical continuum theory of metal spheres.) Therefore, we cannot *a priori* expect the slopes α and β to be predicted correctly from a purely classical theory.

The aim of our present work is a careful reexamination of the size dependence of I and A. We shall first demonstrate that the semiclassical jellium model describes very well the average N dependence of the present available data, even down to very small clusters where A is far from being linear in $N^{-1/3}$, if the (slightly wrongly predicted) bulk limit W is adjusted to the experimental value. We shall then use the semiclassical theory to extract the slope parameters α and β in a unique way; hereby the inclusion of the nonlinear terms in $1/R_I$ in Eqs. (2) and (3) is crucial. Finally, we shall discuss the classical limits of these quantities in the hope to settle once and for all the abovementioned controversy.

Our paper is organized as follows: In Sec. II we discuss the experimental determination of ionization potentials and electron affinities. In Sec. III we briefly summarize the semiclassical density variational method and present some typical results of our calculations. In Sec. IV these are systematically compared to experimental values of I and A. We then address in Sec. V the question of the asymptotic behavior of I and A for large N and discuss the classical limit of the density variational theory. A short summary is presented, as usual, in the last section (Sec. VI).

II. EXPERIMENTAL DETERMINATION OF IONIZATION POTENTIALS AND ELECTRON AFFINITIES

A number of techniques are used for the determination of cluster ionization potentials I. Most frequently, electron impact or light irradiation serve to ionize the species; the observed quantity usually is the resulting ion current, measured as function of electron or photon energy. Other techniques employ energy resolved electron detection (photoelectron spectroscopy) with simultaneous detection of the corresponding ions. The experiments are performed on mass-unselected beams, i.e., on a mixture containing different sizes and often even different materials. Therefore, mass analysis is necessary after the ionization process. In cases where the clusters dissociate upon ionization, an unambiguous assignment of the ionization signal to a defined cluster size might be difficult or even impossible. Especially with energies far beyond the ionization threshold, the electronic excess energy could relax into high vibrationally excited ionic states, thus leading to fragmentation before the ion is detected. The determination of I by photoionization mass spectroscopy with photon energies near threshold is not affected by this problem, as long as the ionization potentials are monotonously decreasing with increasing cluster size.

Electron affinities A, on the other hand, are determined with negatively charged clusters. Here, the additional charge allows a mass selection with electric and/or magnetic fields *prior* to the measurement. When, in addition, the negative clusters grow directly in the source and undergo a supersonic expansion, low-temperature (i.e., ground-state) mass-selected clusters are prepared. Monochromatic light irradiates the clusters and detaches electrons, their energy being analyzed in an electron spectrometer. Strictly speaking, these experiments determine the *electron detachment energies* rather than A. Note that the detachment experiments inquire the binding energy of an electron to an anion in its charged ground state, and not the electron attachment energy to a neutral ground-state cluster. Only in cases where the ground-state geometries of the neutral and the corresponding negatively charged clusters are identical, a photodetachment experiment directly gives the (adiabatic) electron affinity.

All ionization energies and electron affinities discussed in this communication have been measured by photoionization (PI), or by photodetachment (PD). Generally, such experiments explore vertical transitions, thus yielding vertical ionization potentials and vertical detachment energies. In some cases, however, the corresponding adiabatic energies can be estimated from the shapes of the curves near

threshold. In small molecules, the threshold behavior is mainly determined by the electronic vibrational coupling and by the internal energy. In the absence of low-lying electronically excited neutral or ionic states, PI thresholds can in principle be calculated from the ground state properties.[28] In metal clusters, on the other hand, the interpretation of threshold behavior and especially the assignment of I and A values is controversial. A number of factors complicate the situation—the density of electronic states, isomeric structures, the electronic vibrational coupling, low-lying excited states, etc. Standard approaches as used for polyatomic molecules (Watanabe plots,[29] extrapolation to zero signal, and step function fit procedures) have been applied to derive I values. Limberger and Martin[30] use a model of displaced harmonic oscillators to assign vertical ionization potentials. So far, no method seems to be suited to explain all features of PI and PD thresholds. In many cases, very long tails are found rather than distinct thresholds. For small clusters, the measured PI and PD energies might significantly differ (by up to several hundred meV) from the respective I and A values. With increasing size, this effect is expected to decrease.

Here we will use PI threshold values given by the various authors, as listed in Table I. For the PD thresholds, the authors also use different procedures and give either estimates of vertical, adiabatic, or upper limits of adiabatic detachment energies. In many cases, the data severely depend on the authors' view which might place the detachment threshold in a wide range. For consistency, we define the threshold energies as the onset of the electron signal above background fixed at a given percentage of the peak intensity (see Table I) corrected by the instrumental broadening. Due to a lack of better knowledge, the resulting PD and PI energies will be taken as A and I values for our comparison between theory and experiment. At present, more elaborate methods of threshold determination do not appear useful, since the physical origin of the near-threshold spectral shapes is still unclear.

III. SEMICLASSICAL DENSITY VARIATIONAL JELLIUM MODEL FOR SPHERICAL METAL CLUSTERS

Let us briefly summarize the recently developed[14] semiclassical density variational method which we employ here for our theoretical calculations. According to density functional theory,[49] we write the total energy of the cluster as a functional of the local density $\rho(\mathbf{r})$ of the valence electrons

$$E[\rho] = \int \left\{ \tau[\rho(\mathbf{r})] + \mathscr{E}_{\rm xc}[\rho(\mathbf{r})] + \frac{1}{2} e^2 \rho(\mathbf{r}) \times \left[\int \frac{\rho(\mathbf{r}')}{|\mathbf{r}-\mathbf{r}'|} d^3r' \right] + V_I(\mathbf{r})\rho(\mathbf{r}) \right\} d^3r + E_I. \tag{5}$$

TABLE I. Sources of experimentally determined metal cluster ionization potentials and electron affinities. Photoionization (PI), photodetachment (PD).

	References	Methods	Data used here (method, N range)
Na_N I	Herrmann *et al.* (31)	PI, step function	
	Kappes *et al.* (32)	PI, linearization, Watanabe, pseudo-Watanabe	pseudo-Watanabe, 3–22
	Honea *et al.* (33)	PI, bracketing	40, 58, 91, 137
K_N I	Herrmann *et al.* (31)	PI, step function	
	Saunders (34), Cohen *et al.* (35)	PI, linearization	3–21, 23–32, 34, 36, 38–44, 46–48, 50–52, 54, 56–66, 68–76, 78, 80, 82, 84, 86, 88, 90–96, 100, 101
	Bréchignac *et al.* (36)	PI, linearization	
	Kappes *et al.* (37)		
Cu_N A	Leopold *et al.* (19)	PD	3–5, 7–10
	Ho *et al.* (38)		
	Pettiette *et al.* (39)	PD, significant onset	11–41
	Ganteför (40)	PD, 3% above threshold	6
	Cheshnovsky *et al.* (41)	PD, significant onset	121, 193, 256, 342, 410
Ag_N A	Ganteför *et al.* (20, 42)	PD, 5% above threshold	3–16, 18–21
	Ho *et al.* (38)	PD, 10% above threshold	
In_N A	Gausa *et al.* (21)	PD, 1.5% above threshold	3–18
Tl_N A	Gausa *et al.* (21)	PD, 1.5% above threshold	3–20
Al_N I	Jarrold *et al.* (43)	Collision-induced fragmentation (CIF)	
	Begemann *et al.* (44)	CIF	
	Schriver *et al.* (45)	PI, linearization	3–70
Al_N A	Ganteför *et al.* (46)	PD, 3% above threshold	3–22
	Taylor *et al.* (47)	PD, 3% above threshold	23–32
	Lüder *et al.* (48)	PD, 3% above threshold	40, 60, 70, 120, 150

Here $\tau[\rho]$ and $\mathscr{E}_{xc}[\rho]$ are the kinetic and the exchange-correlation energy densities, respectively. (For the latter, we use the LDA functional of Gunnarsson and Lundqvist.)[50] The third term in Eq. (5) is the Hartree–Coulomb energy of the valence electrons; $V_I(\mathbf{r})$ is the potential and E_I the total electrostatic energy of the positive ionic jellium background. The latter is defined as usual by a sphere of radius R_I [see Eq. (4)] with constant density $\rho_I = 3/(4\pi r_s^3)$. The density $\rho(\mathbf{r})$ is normalized to the number Z of valence electrons

$$\int \rho(\mathbf{r}) d^3r = Z = wN + z, \tag{6}$$

where w is the valence factor ($w = 1$ for monovalent atoms, etc.) and z the number of excess electrons.

Expressing ρ and τ through single-particle wave functions ϕ_i and varying $E[\rho]$ with respect to the ϕ_i leads to the Kohn–Sham equations which have been solved for spherical,[5,6,9,11] spheroidal,[7] and triaxially deformed[51] clusters. Alternatively, semiclassical gradient expansions[49,52] of $\tau[\rho]$ can be employed in order to vary directly the density $\rho(\mathbf{r})$, either by solving the corresponding Euler variational equation,[26] or using trial density functions.[3,14,25,27,53]

We choose[14] to perform a restricted variation of the spherical densities $\rho(r)$, parametrizing them by the following trial function:

$$\rho(r) = \rho_0 \left[1 + \exp\left(\frac{r-R}{a} \right) \right]^{-\gamma}. \tag{7}$$

The total energy (5) for a cluster with given N and Z is then minimized with respect to the parameters ρ_0, R, a, and γ subject to the constraint (6). [Note that the parameter γ regulates the asymmetry ($\gamma \neq 1$) of the density surface profile around its inflection point; typical values are $\gamma \simeq 0.4$–0.6 for most clusters.] We utilize hereby the gradient-expanded functional $\tau_{\mathrm{ETF}}[\rho]$ of the extended Thomas–Fermi (ETF) model including all terms up to fourth order.[52] This functional has been shown [54] to reproduce very accurately the average—or semiclassical—part of the kinetic energy of a system of fermions in various types of local potentials, in particular also in nuclei whose densities resemble very much those of the valence electrons in the jellium model.

By this restricted semiclassical variational procedure, we find densities, potentials, and energies which, of course, exhibit no shell effects, but reproduce very closely[14] the *averaged* results of earlier microscopic Kohn–Sham calculations.[5,6] The same method was applied recently[25] to calculate surface energies and bulk work functions for metal surfaces. The results reproduced rather accurately those of similar calculations[55] using the same functional $\tau_{\mathrm{ETF}}[\rho]$, but solving numerically the full Euler variational equation for the electron density. The agreement between these results confirms the good quality of our density parametrization (7).

In Fig. 1, we show a typical result for the two quantities I and A of Na clusters ($w = 1$, $r_s = 3.96$ a.u.) plotted vs $N^{-1/3}$. On the left-hand side, we indicate by an arrow the theoretical bulk work function W [see Eq. (15) in Sec. V B for its definition]. Both I and A are seen to approach W for $N^{-1/3} \to 0$. We find that this holds for all metallic values of

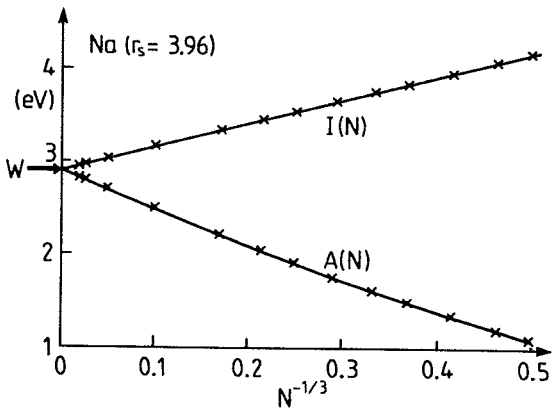

FIG. 1. Ionization potential I and electron affinity A calculated in our semiclassical ETF model for spherical Na clusters with $8 \leq N \leq 125\,000$ plotted versus $N^{-1/3}$. Shown on the left is the theoretical bulk work function W [Eq. (15)] (r_s is in a.u.).

r_s (see also Table II in Sec. V below), thus having achieved a numerical improvement over similar older results[3,53] in which less flexible density profiles were used and $\tau_{\mathrm{ETF}}[\rho]$ was truncated at second order. Note that I here is almost linear in $N^{-1/3}$ even for small clusters, whereas A has a clear curvature due to the term $\propto O(R_I^{-2})$ in Eq. (3). We shall demonstrate in Sec. IV that such nonlinear behavior, which depends on the metal via r_s, can indeed be seen in the experimental quantity A and, to a lesser extent, for some metals also in I.

It becomes obvious from the results in Fig. 1 that our ETF results are ideal for determining the slope parameters α and β in the asymptotic expressions (2) and (3). We shall come back to their accurate determination and discussion in Sec. V. Our first goal, in Sec. IV, will be the comparison of the ETF results with experimental data.

IV. COMPARISON OF ETF RESULTS TO EXPERIMENTALLY DETERMINED THRESHOLD ENERGIES

The tools outlined above are now applied to some alkali, coinage metal, and group III cluster systems. Only one parameter, the Wigner–Seitz radius r_s, serves (besides the valence factor w) to characterize the different materials. Instead of presenting the theoretical results for the selected clusters studied experimentally, Figs. 2–5 depict the calculated smooth curves $I(N^{-1/3})$ and $A(N^{-1/3})$, obtained up to maximum sizes of $N \simeq 10^5$, besides the experimental values. As is well known for the jellium model without ionic structure,[56] the calculated bulk work functions W are typically ~ 0.5–1 eV below the experimental values W_{bulk} of polycrystalline materials. Therefore, in Figs. 2–5, the absolute positions of the curves are adjusted to reproduce the experimental values [57] of W_{bulk}.

For I, the calculations yield very weak curvatures, whereas for A the slopes significantly depend on N. This behavior is throughout followed by the measured cluster PI and PD threshold energies (see the rhombic symbols in Figs.

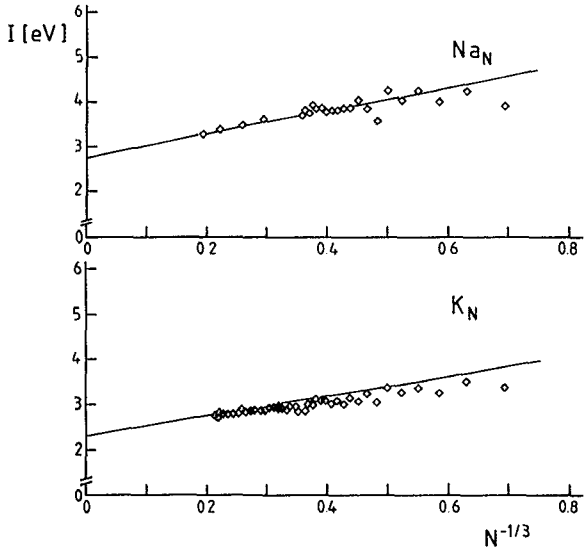

FIG. 2. Full line: ETF results for Na_N ($r_s = 3.96$ a.u., $w = 1$) and K_N ($r_s = 4.86$ a.u., $w = 1$) ionization energies I. At $N^{-1/3} = 0$, the curves are adjusted to the measured bulk work functions of the corresponding polycrystalline materials. Square symbols: experimental values (see Sec. II).

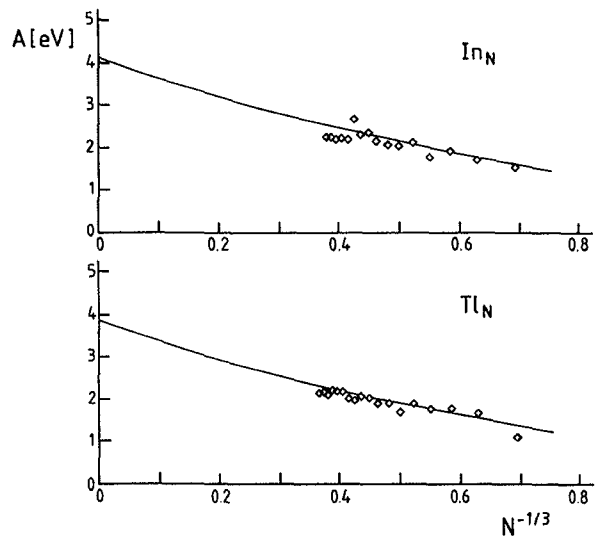

FIG. 4. The same as Fig. 3, but for In_N ($r_s = 3.47$ a.u., $w = 1$) and Tl_N ($r_s = 3.59$ a.u., $w = 1$).

2–5). Note that the ETF and the measured results can directly be compared, i.e., no determination of a cluster radius is necessary since we plot them directly vs $N^{-1/3}$, in contrast to most of the earlier analyses.[17,19–21]

In Figs. 2 and 4, an excellent agreement is observed between theory and the mean experimental results. The measured data of Ag_N, Cu_N, and Al_N partially scatter around the calculated curve, but also show several pronounced discontinuities in their N dependencies. In extreme cases, the calculated energy departs by about 1 eV from the measured threshold [cf. $A(Cu_{20}$, Fig. 3)]. As has been discussed above, the present ETF results are obtained in a *spherical* jellium without shell effects. From recent discussions,[1,7,58] it is well known that nonclosed-shell clusters tend to find their energy minima in deformed geometries. Our theory turns out to work best for closed-shell clusters, i.e., for systems with 8, 18, 20, 40, ... electrons. In the case of negatively charged monovalent atom clusters (see Fig. 3), closed shells are expected at $N = 7, 17, 19, 39, \ldots$. Again, at these sizes the measured threshold energies are shown to be very close to the ETF result. Similar shell effects are observed for aluminum (Fig. 5). Here, the steps coincide with the jellium model when each Al atom is considered to contribute three valence electrons.

So far the absolute positions of the calculated curves were adjusted to the experimental values W_{bulk}. If one takes the *difference* $I - A$, the asymptotic bulk value cancels

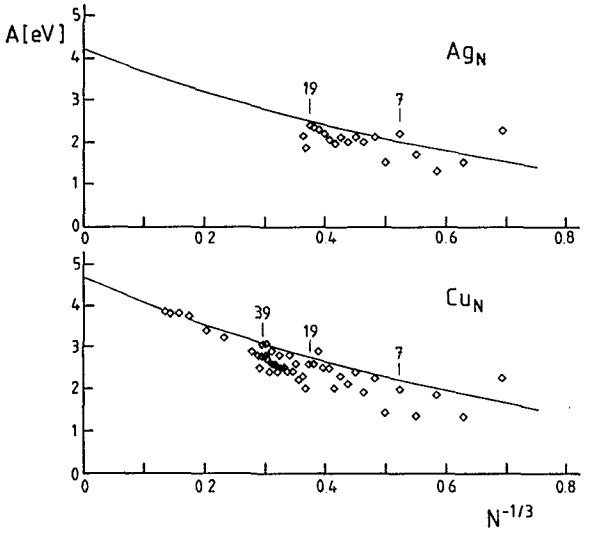

FIG. 3. ETF results compared to measured photodetachment energies (as estimates of A values) for Ag_N ($r_s = 3.03$ a.u., $w = 1$) and Cu_N ($r_s = 2.67$ a.u., $w = 1$). Closed-shell clusters are indicated by their atomic numbers N.

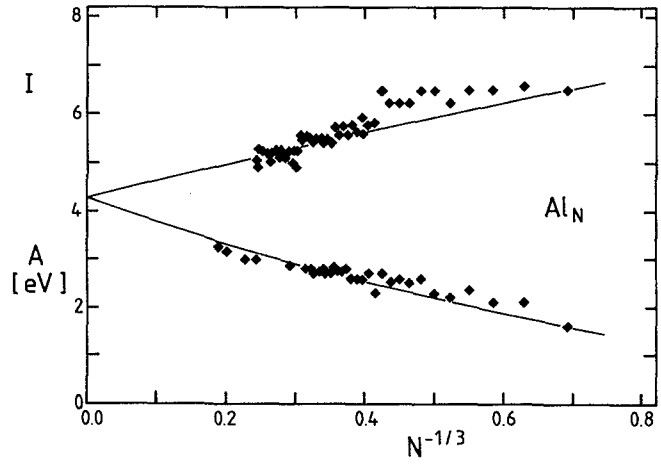

FIG. 5. Calculated and measured I and A for Al_N ($r_s = 2.99$ a.u., $w = 3$).

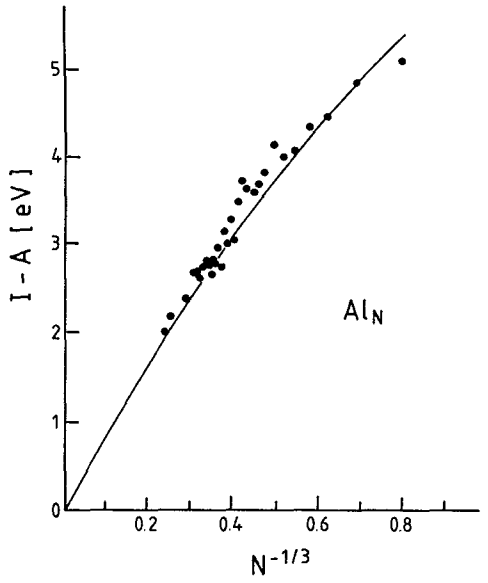

FIG. 6. Calculated (full line) and measured differences $I - A$ for Al_N.

according to Eqs. (2) and (3) with $W_I = W_A = W$. Figure 6 compares the calculated values of $I - A$, *without any adjustment of their vertical position*, to the respective measured differences for aluminum clusters Al_N. The curvature in the $N^{-1/3}$ dependence of the measured results again is well reproduced by the theory even down to small cluster sizes. This underlines that the jellium model correctly reproduces the measured average size dependencies of I and A, irrespective of the wrongly predicted bulk work functions. This result gives some justification of our *ad hoc* adjustment of the bulk values W in the previous figures.

As we shall see in the next section, the slopes α and β with which the curves in Figs. 1–5 reach the bulk values W [see Eqs. (2) and (3)] are not the same for all metals, but depend on the Wigner–Seitz radius r_s. Unfortunately, there are too few precise enough measurements available for sufficiently large clusters, where these slopes are reached asymptotically, for an experimental verification of this r_s dependence.

V. ASYMPTOTIC BEHAVIOR OF I AND A AND DISCUSSION OF THE CLASSICAL LIMIT

We now address the question of the asymptotic limiting behavior of I and A as the cluster size tends to infinity. As we have seen in Sec. III (Fig. 1), our ETF variational results have the correct theoretical bulk value W. Since we can easily calculate clusters with $N \simeq 10^6$, our method provides an ideal tool for a systematic investigation of the coefficients in the asymptotic expressions (2) and (3). Some preliminary results of this analysis have recently been presented;[25,59] a more detailed theoretical investigation will be presented in a forthcoming publication.[60]

A. Determination of the slope parameters α and β

By least-squares fits to $I(N)$ and $A(N)$ for $1000 \leqslant N \leqslant 125\,000$, we have determined the quantities W_I, W_A, α, and β in the asymptotic expressions (2) and (3) as four independent parameters. The results are given in Table II for a series of r_s values. As has to be expected from theoretical considerations (see Sec. V B), W_I and W_A are identical within a high accuracy; they furthermore agree with the theoretical bulk value W (15) to within four decimals. This not only tests the consistency of our model, but represents, as already mentioned in Sec. III, a considerable improvement over earlier similar analyses.[3,53]

TABLE II. Parameters in the asymptotic expansions (2) and (3) of ionization potential and electron affinity, determined from the full variational ETF results by least-squares fit (see the text). W is the theoretical bulk work function (15) calculated for an infinite plane surface.

r_s (a.u.)	W_I (eV)	W_A (eV)	W (eV)	α	β
2.0	3.613	3.611	3.612	0.423	0.569
3.0	3.252	3.251	3.252	0.410	0.587
4.0	2.885	2.885	2.885	0.398	0.601
5.0	2.569	2.569	2.569	0.387	0.612
6.0	2.303	2.303	2.303	0.380	0.619

Let us emphasize once again that different from other experimental[17–21] and theoretical[24,27] analyses, we do *not* include in the leading finite-size terms $\propto N^{-1/3}$ any correction for the electronic spillout over the jellium edge. Such corrections are contained in the higher-order terms $O(R_I^{-2})$. In our opinion, the use of any effective radius R, taking into account the electronic spillout, instead of R_I, renders the experimental determination of α and β doubtful because there is (so far) no unique way to determine experimentally such a cluster radius. On the other hand, if a constant is added to R_I, the resulting values of the slope parameters become model dependent. From the figures in Secs. III and IV, it also becomes evident that the terms $O(R_I^{-2})$ in Eqs. (2) and (3) are indispensible for extracting unique values of the slope parameters.

Our values of α and β are *asymptotic* in the sense that they give the slopes of I and A with respect to $N^{-1/3}$ strictly in the limit $N \to \infty$. To the extent that the curves in Figs. 1–5 are not linear, these values therefore do *not* represent the average slopes. This must be borne in mind when comparing to the slopes of fits to experimental results in the domain of small clusters, where the curvature terms $O(R_I^{-2})$ might play an important role, as shown above in some instances.

Note that α and β in Table II have a weak, but systematic dependence on r_s, i.e., on the electron density. For $r_s \gtrsim 5$ a.u. they are close to the values $\frac{3}{8}$ and $\frac{5}{8}$, respectively, used by many authors who refer to classical *image charge* arguments.[15,16–18,22] This approximate agreement is, however, *accidental*. In fact, as already pointed out in the literature[23–26] and as we will discuss again in Sec. V B, the contribution of the Coulomb energy alone would lead to $\alpha = \beta = \frac{1}{2}$ in a classical continuum limit. The differences from the value $\frac{1}{2}$ are due to *quantum-mechanical* effects, i.e., to the kinetic, exchange, and correlation energies and the fact that the electron density has a quantum-mechanical tail (spillout).

(Note, however, that the sum of α and β is close to unity for all values of r_s, in agreement with some theoretical arguments.)[26]

B. Discussion of the classical limits of I and A

As already mentioned in the Introduction, there exists in the literature a confusing controversy about the classical values to be expected for I and A in the limit of very large clusters.[12,16,22-27] In order to elucidate this point, let us consider the classical limit of our calculations. By definition, the classical limit consists of considering only the classical Coulomb terms in the total energy (5) and omitting the kinetic, exchange, and correlation energies. The *exact variational solution* of this classical problem yields[59,60] a square density for the Z valence electrons

$$\rho^{\rm cl}(r) = w\rho_I \Theta(R_e - r), \quad R_e = r_s (Z/w)^{1/3} \tag{8}$$

for the case of a neutral or positively ionized cluster ($Z \lesssim wN$). This corresponds to distributing the positive excess charge *homogeneously* over the volume contained between the two spheres with radii R_I and R_e. Negatively ionized clusters do not exist in this limit since excess electrons cannot be bound classically. The total classical Coulomb energy then becomes (in order to simplify the notation, the second argument of the energy is in the following the *total* number Z of electrons)

$$E_C^{\rm cl}(N,Z) = \frac{3}{5}\frac{e^2}{r_s}\left[\frac{3}{2}Z^{5/3} + (wN)^{5/3} - \frac{5}{2}Z(wN)^{2/3}\right] \quad (Z \lesssim wN). \tag{9}$$

This leads with Eq. (1) to the *classical limit* of the first ionization potential

$$I^{\rm cl} = \frac{e^2}{2R_I} + O(R_I^{-4}). \tag{10}$$

To leading order, this coincides with the naive classical spherical-capacitor model, yielding $I_0^{\rm cl} = e^2/2R_I$, but this simple spherical-capacitor model also gives a result $A_0^{\rm cl} = -e^2/2R_I$ for the electron affinity, because classical electrostatics assumes that excess electrons can be bound in the same way as an excessive positive charge, which means that there must be a certain potential barrier for the electrons at the metal surface. Because such a potential barrier can only arise from quantum-mechanical effects, this model is, strictly speaking, not a purely classical one—in spite of its simplicity. Indeed, if we include all quantum-mechanical terms in the energy function (5), our calculations yield [see Eq. (13) below] a corresponding "classical part" of the electron affinity

$$A^{\rm cl} = -\frac{e^2}{2R_I} + O(R_I^{-4}). \tag{11}$$

The leading term in both expressions (10) and (11) is just the classical charging energy of a metal sphere with the charge $\pm e$ sitting as an infinitely thin film on its surface. It implies the classical values $\alpha = \beta = \frac{1}{2}$, which already have been derived from density variational theory,[23,24] although in somewhat different ways.

Note that there is no finite limit of $I^{\rm cl}$ and $A^{\rm cl}$ for $N \to \infty$, implying that $W^{\rm cl} = 0$. Indeed, the nonzero value of the bulk work function W is entirely due to quantum-mechanical effects, as is well known and can be seen again further below.

The *image charge method*[15,16,22] yields, after subtracting two infinities from each other, the contradicting classical values $\alpha = \frac{3}{8}$ and $\beta = \frac{5}{8}$. We do not need to repeat here the arguments of two recent publications[23,24] in which the image charge method has been analyzed at length and shown, convincingly enough, to be physically unsound, because the classical concept of the image force breaks down at distances of atomic dimensions. In our opinion, the popularity of the image charge results $\alpha = \frac{3}{8}$, $\beta = \frac{5}{8}$ can only be understood by their approximate agreement with some of the experimentally fitted values (at least in the lighter alkalis). As already stated, this partial agreement is a pure accident. Indeed, we have already shown in Sec. IV that the same density functional theory which yields the above (and only sound) classical slopes $\alpha = \beta = \frac{1}{2}$, in its full quantum-mechanical form (even semiclassically) explains the experimental slope parameters to the extent that these can be asymptotically determined. In the following, we shall briefly indicate the origin of the deviations of α and β from the value $\frac{1}{2}$. (For a parallel investigation within the same framework, but using a different line of arguments, see Ref. 26.)

Taking into account the kinetic and exchange-correlation contributions to the total energy (5) and allowing for an exponential tail of the electron density, i.e., *including all quantum-mechanical corrections*, leads to substantial changes in the results (8)–(11), indeed. From a liquid-drop model (LDM) expansion of the *total* semiclassical ETF energy $E(N,Z)$ to be discussed in detail in a forthcoming publication,[60] we find the following leading terms:

$$E(N,Z) = E_C^{\rm cl}(N,Z) + (wN - Z)\Delta\varphi^{\rm out} + e_b Z + (\text{surface terms} \propto Z^{2/3}, N^{2/3}) + \dots . \tag{12}$$

The first term (which is zero for neutral clusters) is just the classical Coulomb energy given in Eq. (9) for $Z \lesssim wN$. In the case $Z \gtrsim wN$, which is now possible due to the binding effects of the exchange and correlation contributions, one has to interchange wN and Z in Eq. (9), yielding the expression

$$E_C^{\rm cl}(N,Z) = \frac{3}{5}\frac{e^2}{r_s}\left[\frac{3}{2}(wN)^{5/3} + Z^{5/3} - \frac{5}{2}wNZ^{2/3}\right] \quad (Z \gtrsim wN) \tag{13}$$

from which one immediately gets Eq. (11). In Eq. (12), $\Delta\varphi^{\rm out}$ is the outer part of the Coulomb barrier of an infinite plane metal surface, i.e., its electrostatic potential φ taken between an infinite distance outside the metal and the jellium edge

$$\Delta\varphi^{\rm out} = \varphi(\infty) - \varphi(0) = 4\pi e^2 \int_0^\infty u\delta\rho(u)du, \tag{14}$$

where $\delta\rho(u) = \rho(u) - \rho_{I0}\Theta(-u)$ and u is the distance from the jellium edge along the normal to the surface. [$\Delta\varphi^{\rm out}$ is zero in the classical limit where $\rho(u)$ is also a step

function.] Finally, e_b in Eq. (12) is the bulk energy per electron, which consists exclusively of the quantum-mechanical kinetic, exchange, and correlation energies.

From Eq. (12), one finds easily the asymptotic expressions (2) and (3) for I and A, whereby $W_I = W_A = W$ is given by

$$W = \Delta\varphi^{\text{out}} - e_b \tag{15}$$

in agreement with Mahan and Schaich.[61]

The classical contribution to I and A is given by Eqs. (10) and (11). However, the surface terms $\propto Z^{2/3}$ in Eq. (12) contribute *at the same order* $1/R_I$ to I and A, thus changing the slope parameters α and β from their classical value $\frac{1}{2}$. The analytic form of these surface contributions is being studied presently.[60] The final numerical values of the slope parameters are given numerically in Table II.

With this short outline of the formal LDM expansion of the average energetics of metal clusters,[60] we hope to have made it clear that the deviation of the slope parameters α and β from their correct classical values $\frac{1}{2}$ are, in fact, due to quantum-mechanical effects. Their approximate agreement, both in experiment and in our variational ETF theory, with the values $\frac{3}{8}$ and $\frac{5}{8}$ should therefore not be taken as support for the incorrect values found with the image charge potential.[15,16,22] (See, also, Ref. 62.)

VI. SUMMARY

By way of a summary, we list here the main points of our findings.

(1) The average ionization potentials I and electron affinities A are, in general, *nonlinear* in $N^{-1/3}$. This can be clearly recognized in the experimental results, especially in the electron affinities.

(2) In many cases, experimental values of I and A are only known for small clusters where this nonlinearity becomes important and a straight-line fit in terms of $N^{-1/3}$ therefore *cannot* be extrapolated to the bulk work function W for $N^{-1/3} \to 0$.

(3) Apart from the well-known shift in the constant W, the (semiclassical ETF) jellium model is able to correctly reproduce the average size dependence of the experimental I and A of many simple metals, in particular also for smaller clusters where the nonlinearity in $N^{-1/3}$ is clearly observable.

(4) The slope parameters α and β in the asymptotic expressions (2) and (3) differ from the value $\frac{1}{2}$ which results uniquely (together with $W^{\text{cl}} = 0$) from density functional theory in the classical limit.

(5) The deviations of α and β from the value $\frac{1}{2}$, which depend slightly on r_s, are explained in density functional theory by quantum-mechanical effects (kinetic, exchange, and correlation energies, and the diffuseness of the electron density). We recall that it is exactly the same effects which cause the finite value of the bulk work function W.

ACKNOWLEDGMENT

Work supported by Deutsche Forschungsgemeinschaft.

[1] W. A. de Heer, W. D. Knight, M. Y. Chou, and M. L. Cohen, Solid State Phys. **40**, 93 (1987).
[2] T. H. Upton, Phys. Rev. Lett. **56**, 2168 (1986); B. K. Rao, S. N. Khanna, and P. Jena, NATO ASI Series B **158**, 369 (1987); V. Bonačić-Koutecký, P. Fantucci, and J. Koutecký, J. Chem. Phys. **93**, 3802 (1990); I. Moullet, J. L. Martins, F. Reuse, and J. Buttet, Phys. Rev. Lett. **65**, 476 (1990).
[3] M. Cini, J. Catalysis **37**, 187 (1975).
[4] J. L. Martins, R. Car, and J. Buttet, Surf. Sci. **106**, 265 (1981).
[5] W. Ekardt, Phys. Rev. B **29**, 1558 (1984).
[6] D. E. Beck, Phys. Rev. B **30**, 6935 (1984).
[7] W. Ekardt and Z. Penzar, Phys. Rev. B **38**, 4273 (1988); Z. Penzar and W. Ekardt, Z. Phys. D **17**, 69 (1990).
[8] S. Bjørnholm, J. Borggreen, O. Echt, K. Hansen, J. Pedersen, and H. D. Rasmussen, Phys. Rev. Lett. **65**, 1627 (1990).
[9] T. P. Martin, T. Bergmann, H. Göhlich, and T. Lange, Phys. Rev. Lett. **65**, 748 (1990); *International Symposium on Small Particles and Inorganic Clusters (ISSPIC5)*, edited by O. Echt and E. Recknagel (Springer, Berlin, 1991).
[10] H. Nishioka, K. Hansen, and B. R. Mottelson, Phys. Rev. B **42**, 9377 (1990).
[11] M. Brack, O. Genzken, and K. Hansen, *International Syumposium on Small Particles and Inorganic Clusters (ISSPIC5)*, edited by O. Echt and E. Recknagel (Springer, Berlin, 1991); Z. Phys. D. (in press).
[12] *Small Particles and Inorganic Clusters*, edited by C. Chapon, M. F. Gillet and C. R. Henry (Springer, Berlin, 1989).
[13] *International Symposium on Small Particles and Inorganic Clusters* (ISSPIC5), edited by O. Echt and E. Recknagel (Springer, Berlin, 1991).
[14] M. Brack, Phys. Rev. B **39**, 3533 (1989).
[15] J. M. Smith, Am. Inst. Aeronaut. Astronaut. J. **3**, 648 (1965).
[16] D. M. Wood, Phys. Rev. Lett. **46**, 749 (1981).
[17] E. Schumacher and M. Kappes, in *Large Finite Systems*, edited by J. Jortner, A. Pullmann, and B. Pullmann (Reidel, Dordrecht, 1987), p. 289.
[18] C. Bréchignac, Ph. Cahuzac, F. Carlier, M. de Frutos, and J. Leygnier, J. Chem. Soc. Faraday Trans. **86**, 2525 (1990); Phys. Rev. **63**, 1368 (1989).
[19] D. G. Leopold, J. H. Ho, and W. C. Lineberger, J. Chem. Phys. **86**, 1715 (1987).
[20] G. Ganteför, M. Gausa, K. H. Meiwes-Broer, and H. O. Lutz, Faraday Discuss. Chem. Soc. **86**, 197 (1988).
[21] M. Gausa, G. Ganteför, H. O. Lutz, and K. H. Meiwes-Broer, Int. J. Mass Spectrosc. Ion Proc. **102**, 227 (1990).
[22] M. P. J. van Staveren, H. B. Brom, L. J. de Jongh, and Y. Ishii, Phys. Rev. B **35**, 7749 (1987).
[23] G. Makov, A. Nitzan, and L. E. Brus, J. Chem. Phys. **88**, 5076 (1988).
[24] J. P. Perdew, Phys. Rev. B **37**, 6175 (1988); in *Condensed Matter Theories*, edited by J. Keller (Plenum, New York, 1989), Vol. 4, p. 149.
[25] M. E. Spina, M. Seidl, and M. Brack, in *Symposium on Atomic and Surface Physics (SASP90)*, edited by T. D. Märk and F. Howorka (Innsbruck University, Innsbruck, 1990), p. 426; *International Symposium on Small Particles and Inorganic Clusters (ISSPIC5)*, edited by O. Echt and E. Recknagel (Springer, Berlin, 1991).
[26] E. Engel and J. P. Perdew, Phys. Rev. B **43**, 1331 (1991).
[27] A. Mañanes, M. Membrado, J. Sañudo, A. F. Pacheco, and L. C. Balbás, *International Symposium on Small Particles and Inorganic Clusters* (ISSPIC5), edited by O. Echt and E. Recknagel (Springer, Berlin, 1991); A. Rubio, L. C. Balbás, and J. A. Alonso, Phys. Status Solidi. B (in press).
[28] J. Berkowitz, *Photoabsorption, Photoionization, and Photoelectron Spectroscopy* (Academic, New York, 1979).
[29] K. Watanabe and J. R. Mottl, J. Chem. Phys **26**, 1773 (1957).
[30] H. G. Limberger and T. P. Martin, J. Chem. Phys. **90**, 2979 (1989).
[31] A. Herrmann, S. Leutwyler, E. Schumacher, and L. Wöste, Helv. Chim. Acta **61**, 453 (1978).
[32] M. M. Kappes, M. Schär, U. Röthlisberger, C. Yeretzian, and E. Schumacher, Chem. Phys. Lett. **143**, 251 (1988).
[33] E. C. Honea, M. L. Homer, J. L. Persson, and R. L. Whetten, Chem. Phys. Lett. **171**, 147 (1990).
[34] W. A. Saunders, Ph.D. thesis, Berkeley, 1986, unpublished.
[35] M. L. Cohen, M. Y. Chou, W. D. Knight, and W. A. de Heer, J. Phys. Chem. **91**, 3141 (1987).
[36] C. Bréchignac and Ph. Cahuzac, Chem. Phys. Lett. **117**, 365 (1985); Z. Phys. D **3**, 121 (1986).
[37] M. Kappes, M. Schär, P. Radi, and E. Schumacher, J. Chem. Phys. **84**, 1863 (1986).
[38] J. Ho, K. M. Erwin, and W. C. Lineberger, J. Chem. Phys. **93**, 6987

(1990).
[39]C. L. Pettiette, S. H. Yang, M. J. Craycraft, J. Conceicao, R. T. Laaksonen, O. Cheshnovsky, and R. E. Smalley, J. Chem. Phys. **88**, 5377 (1988).
[40]G. Ganteför, Ph.D. thesis, University of Bielefeld, 1989, unpublished.
[41]O. Cheshnovsky, K. J. Taylor, J. Conceicao, and R. E. Smalley, Phys. Rev. Lett. **64**, 1785 (1990).
[42]G. Ganteför, M. Gausa, K. H. Meiwes-Broer, and H. O. Lutz, J. Chem. Soc. Faraday Trans. **86**, 2483 (1990).
[43]M. F. Jarrold and J. E. Bower, J. Chem. Phys. **87**, 1610 (1987).
[44]W. Begemann, R. Hector, Y. Y. Liu, J. Tiggesbäumker, K. H. Meiwes-Broer, and H. O. Lutz, Z. Phys. D **12**, 229 (1989).
[45]K. E. Schriver, J. L. Persson, E. C. Honea, and R. L. Whetten, Phys. Rev. Lett. **64**, 2539 (1990).
[46]G. Ganteför, M. Gausa, K. H. Meiwes-Broer, and H. O. Lutz, Z. Phys. D **9**, 253 (1988); G. Ganteför, K. H. Meiwes-Broer, and H. O. Lutz, Phys. Rev. A **37**, 2716 (1988).
[47]K. J. Taylor, C. L. Pettiette, M. J. Craycraft, O. Cheshnovsky, and R. E. Smalley, Chem. Phys. Lett. **152**, 347 (1988).
[48]Ch. Lüder, H. R. Siekmann, and K. H. Meiwes-Broer (to be published).
[49]J. P. Hohenberg and W. Kohn, Phys. Rev. B **136**, 864 (1964); W. Kohn and L. Sham, Phys. Rev. A **140**, 113 (1965).
[50]O. Gunnarsson and B. I. Lundqvist, Phys. Rev. B **13**, 4274 (1976).
[51]G. Lauritsch, P.-G. Reinhard, J. Meyer, and M. Brack (unpublished).
[52]C. H. Hodges, Can. J. Phys. **51**, 1428 (1973).
[53]D. R. Snider and R. S. Sorbello, Phys. Rev. B **28**, 5702 (1983); Solid State Commun. **47**, 845 (1983).
[54]C. Guet and M. Brack, Z. Phys. A **297**, 247 (1980); M. Brack, C. Guet, and H.-B. Håkansson, Phys. Rep. **123**, 275 (1985).
[55]P. Tarazona and E. Chacón, Phys. Rev. B **39**, 10366 (1989).
[56]N. D. Lang and W. Kohn, Phys. Rev. B **3**, 1215 (1971).
[57]*Handbook of Chemistry and Physics*, edited by R. C. Weast (CRC, Boca Raton, Fla., 1988).
[58]K. Selby, M. Vollmer, J. Masui, V. Kresin, W. A. de Heer, and W. D. Knight, Phys. Rev. B **40**, 5418 (1989).
[59]M. Seidl, diploma thesis, University of Regensburg, 1989, unpublished.
[60]M. Seidl, M. E. Spina, and M. Brack (to be published).
[61]G. D. Mahan and W. L. Schaich, Phys. Rev. B **10**, 2647 (1974).
[62]W. A. de Heer and P. Milani, Phys. Rev. Lett. **65**, 3356 (1990).